Bull. Mater. Sci., Vol. 38, No. 2, April 2015, pp. 335–342. © Indian Academy of Sciences.

Effect of electro-co-deposition parameters on surface mechanical properties of Cu–TiO_2 composite coating

AKARAPU ASHOK[1], H S MAHARANA[2] and A BASU[2,*]

[1]Department of Physics, Indian Institute of Technology Hyderabad, Yeddumailaram 502 205, Telangana, India
[2]Department of Metallurgical and Materials Engineering, National Institute of Technology, Rourkela 769008, Odisha, India

MS received 28 May 2014

Abstract. **The present work describes processing and properties of Cu–TiO_2 electrodeposited coating on copper substrate with optimized current density and ultrafine ceramic TiO_2 powder in the plating bath. Direct current electrodeposition process was employed to develop the composite coating with Cu matrix and ceramic oxide (TiO_2) nanoparticles as reinforcement on copper substrate. The coatings were developed with 0 (unreinforced), 10 and 30 g l^{-1} TiO_2 powder in bath, at four different current densities (5, 8, 11 and 14 A dm^{-2}) to study the effect of current density and particle concentration in bath on the structure and properties of the developed coatings. Phase, microstructure and compositional analysis of the coatings were characterized by X-ray diffraction (XRD), scanning electron microscopy (SEM) and energy-dispersive X-ray spectroscopy (EDS), respectively. Hardness and wear resistance of the coatings were analysed by using microhardness tester and ball on plate wear tester and improvement in these properties was observed due to particle reinforcement and crystallographic texture.**

Keywords. **Electrodeposition; electro-co-deposition; TiO_2; copper; texture; microhardness; wear.**

1. Introduction

Copper (Cu) is environment friendly and easily available material that possesses a unique combination of low electrical resistivity (16.78×10^{-9} Ω m) and high thermal conductivity (394 W m^{-1} K^{-1}), excellent malleability, reasonably good corrosion resistance at ambient temperature[1] and recyclability. Owing to these excellent combination of properties Cu and its alloys are most widely used engineering materials for conduction of electricity (electrical conductors, wires, contacts, plugs) and heat (heat exchangers, linings, radiators, electrodes). However, poor mechanical property often necessitates strengthening without adversely affecting its electrical/thermal conductivity. Some applications like electrical contacts require mainly good surface mechanical properties like hardness, wear resistance due to frequent rubbing action during switching. Bulk modification/alloying decreases thermal and electrical conductivity. Along with electrical conductivity, thermal conductivity is also important so that the contacts can quickly release the heat accumulated for resistance heating and rubbing action during switching. In such components surface engineering approach is wise one as it does not adversely affect bulk properties like electrical and thermal conductivities compared to bulk modification. The wide variety of surface coating techniques available are physical vapour deposition, chemical vapour deposition, thermal spraying, electrodeposition, electroless deposition, diffusion coatings and laser-based techniques, etc.

Metal matrix nanocomposites containing dispersed second-phase particulates have various special properties such as dispersion hardening, self-lubricity, high temperature inertness, good wear and corrosion resistance and chemical and biological compatibility.[2–7] Electro-co-deposition has several advantages in developing metal matrix composite coatings among other coating processes such as, uniform depositions on complexly shaped substrates, low cost, good reproducibility and the reduction of waste.[8] Electro-co-deposition process has been in use successfully to develop such nanocomposite coatings from the past decades. The second phase can be hard oxide (Al_2O_3, TiO_2 and SiO_2) or carbide particles (SiC, WC) embedded in metals like Cu, Ni, Cr, Co and various alloys.[7] The applications of these coatings include wear and abrasion resistant surfaces, lubrication, high hardness tools, dispersion-strengthened alloys and for protection against oxidation and hot corrosion.[7,9–11]

The quality of the deposits is influenced by wide number of variables which include current density, particle characteristics, bath composition and the particle–bath interaction. The amount of embedded second phase particles plays an important role in improving the surface mechanical properties by refining the grain size of the matrix and also by dispersion strengthening mechanism. Several parameters affect the embedded volume % of second phase particles, among which current density, particle concentration in the bath and pH of the solution are important variables. Current density plays an important role in controlling the deposition rate which will in

*Author for correspondence (basua@nitrkl.ac.in; anindya.basu@gmail.com)

turn affect the concentration of incorporated particles in the coatings.

The present work was undertaken to explain the mechanism and main factors affecting the incorporation of TiO_2 ultrafine solid particles into copper matrix by electro-co-deposition. The influence of TiO_2 nanoparticles in electrolyte and deposition current density on the coating properties were studied. The results were compared with pure copper coatings to understand the effects of dispersed phase on the properties of composite coatings during electro-crystallization.

2. Experimental

2.1 *Sample preparation*

For the deposition of Cu–TiO_2 composite coatings, copper was selected as substrate material. The substrates were collected from hot rolled copper strip by cutting it into averagely 20 mm × 15 mm × 3 mm size pieces. Then the substrates were mirror polished by belt grinder for oxide layer removal, then on emery papers (1/0, 2/0, 3/0, 4/0), then rough cloth polishing in which Alundum was used as abrasive agent. Finally the substrates were fine polished by fine cloth in which diamond paste was used as polishing agent. Later the substrates were cleaned with soap and then washed with water and rinsed with alcohol. Holes were made on the samples by 2 mm diameter drill bit to dip the samples in the electrolyte solution and to supply current by attaching copper wire to the hole.

2.2 *Plating bath solution preparation*

Parallel plate electrode configuration and copper sulphate bath without the addition of surfactant and additives is used for the codeposition of TiO_2 in the copper matrix. The bath compositions and deposition parameters used for Cu–TiO_2 composite coatings are reported in table 1. The pH of the solution was maintained below the iso-electric point (IEP), so that the particles in the suspension acquire positive charge in the acid solution and get deposited on the cathode metal substrate. Pure copper strip was used as anode and prepared (hot rolled) copper substrates as cathodes. Before deposition the solution was allowed for ultrasonication for 25 min and magnetic stirring for 30 min for homogeneous dispersion of the TiO_2 powder in the solution. Magnetic stirrer was used for stirring of the bath during entire deposition so that the sedimentation of powder particles in the solution is prevented and they can be homogeneously dispersed during deposition in the copper matrix. Pure copper deposits were also done by using the same parameters which was used for TiO_2 deposition for comparison of the results.

Table 1. Electrolytic bath composition and coating parameters.

Electrolyte (acidic copper sulphate bath)	Copper sulphate ($CuSO_4 \cdot 5H_2O$): 200 g l^{-1} Sulphuric acid (H_2SO_4): 50 g l^{-1}
pH	2.17
Current density	5, 8, 11 and 14 A dm^{-2}
Temperature	Room temperature
Plating time	40 min
Dispersion	TiO_2: 0, 10 and 30 g l^{-1} (each at all current density)

2.3 *Characterization*

The phases obtained in the coating and the TiO_2 powder were analysed by Bragg–Brentano (theta–2theta) X-ray diffraction (XRD) using Cu K_α ($\lambda = 0.15406$ nm) radiation in a Philips X-ray diffractometer. Microstructural and compositional studies were carried out by a ZEISS: SUPRA 40 field emission scanning electron microscope (FESEM) equipped with an energy-dispersive X-ray (EDS) detector. Microhardness measurements were carried out on the surface using a Vickers indenter with 5 g load (LECO). Each hardness value reported here is an average of 4–5 measurements on the same sample at equivalent locations. To measure the wear property of the coatings, a ball on plate-type wear testing instrument (DUCOM TR-208-M1) having a hardened steel ball (SAE 52100) indenter of 2 mm diameter was used. Sliding distance *vs*. wear depth of all the coatings were plotted and compared. Surface damage caused by wear testing was subsequently analysed by scanning electron microscopy (SEM) to get an idea about the wear mechanism.

3. Results and discussion

3.1 *Particle size*

Figure 1 shows the particle size distributions of ultrafine TiO_2 powder obtained by using Malvern Zeta sizer. From the figure it can be seen that there are two sharp peaks, which indicate that a range of different sized particles was present

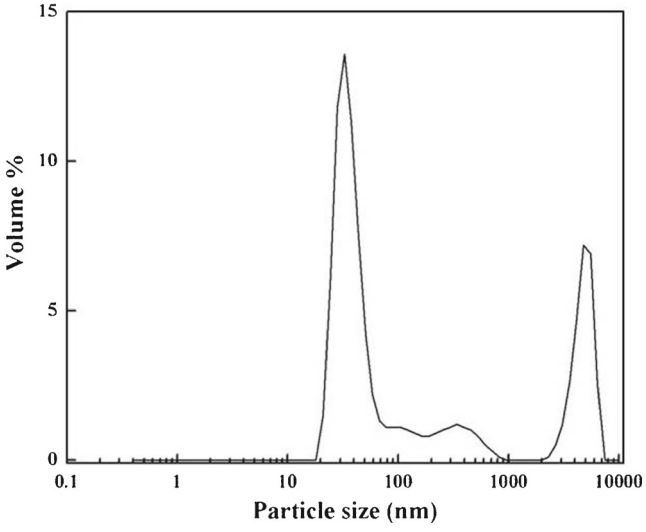

Figure 1. Particle size distribution of procured TiO_2 powder.

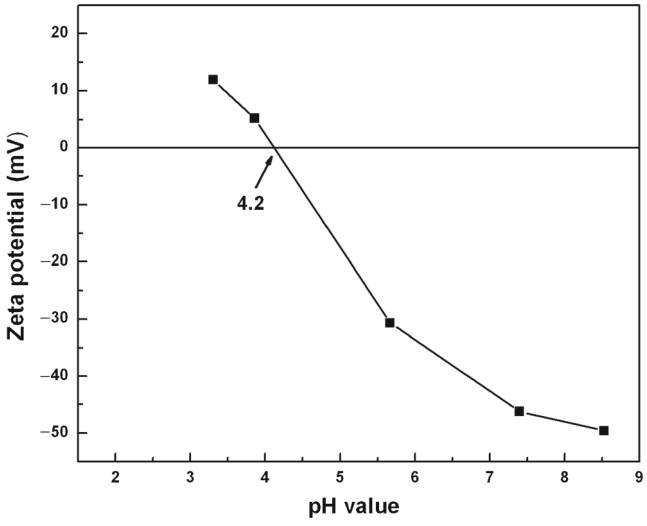

Figure 2. Iso-electric point determination of TiO_2 powder.

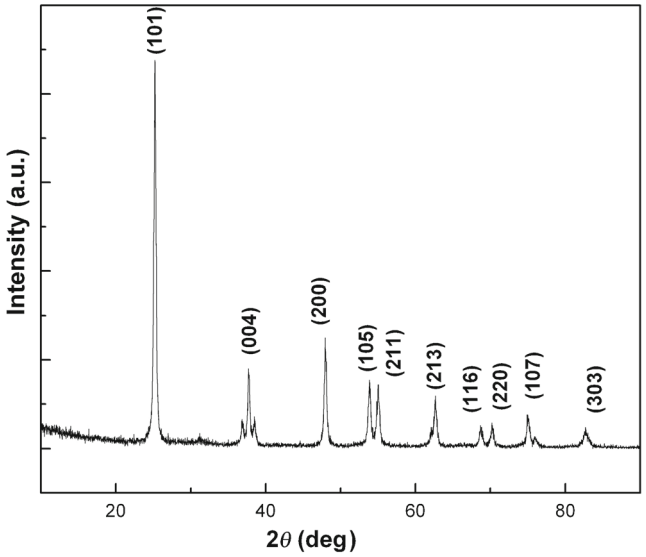

Figure 3. XRD peaks of procured TiO_2 powder.

in the powder. In this case the first peak was observed below 100 nm and the second one was observed above 1 μm. The mean particle size obtained was below 100 nm by cumulative study due to higher volume percentage of particles having sizes within 100 nm.

3.2 *Iso-electric point of TiO_2 powder*

Zeta potential of TiO_2 ultrafine particles in de-ionized water at different pH values was measured to determine the iso-electric point for stable suspension by using Malvern Zeta-sizer instrument prior to the electrodeposition. From figure 2 it can be observed that the IEP of TiO_2 was around 4.2 pH. The pH maintained during the deposition was lower than the obtained iso-electric point, which signifies the acidic nature of the solution and the particles were positively charged in the suspension.

3.3 *XRD analysis*

X-ray diffractograms of all developed coatings and copper substrate were obtained by using Philips X'Pert System. Figure 3 shows the XRD pattern of procured TiO_2 powder. It was confirmed to be tetragonal crystal structure by assigning all diffraction peaks of TiO_2 powder. But there is no appreciable peak broadening observed though the crystallite sizes of powder are in nanometric size. The powder source was confirmed to be synthesized by a chemical route which does not introduce any strain in the powder material. So, the broadening observed was only due to the fine crystallite size, not due to the strain. Figure 4 shows the XRD patterns of Cu–TiO_2 coatings obtained with 10 and 30 g l^{-1} TiO_2 both at different current density along with XRD pattern of the substrate (hot rolled copper). From figure 4 it is evident that all the peaks were belonging to Cu. Although TiO_2 is present in all Cu–TiO_2-coated samples as evidenced from the EDS result, but no peak of TiO_2 was clearly observed probably because of its presence in minor fraction in the composite coating. However, when such diffraction profile was enlarged then it was visible. As example, TiO_2 (anatase type, JCPDS card no: 84-1285) peaks are observed as shown in figure 5 at 2θ angles of 25.24°, 48.0° in Cu–TiO_2 coatings deposited with 10 g l^{-1} TiO_2 and 8 A dm^{-2} current density.

The crystallite size of the deposited Cu of all the coated samples was calculated by using the Scherrer formula given by Equation (1) and the values are listed in table 2. The Scherrer equation can be written as

$$D = \frac{0.94\lambda}{\beta \cos\theta}, \tag{1}$$

where D the crystallite size, β the full-width at half-maximum (FWHM) of the diffraction peak, λ the wavelength of the incidental X-ray (1.54 Å) and θ the diffraction angle. The crystallite sizes of Cu in all deposited samples were found to be less than 100 nm (table 2) and there is no such trend with deposition parameter.

From figure 4 it can also be observed that relative intensities of the different planes change with deposition parameter and bath concentration and it could have pronounced effect on the mechanical properties of the coatings. Hence, for systematic and quantified study of the same relative texture coefficient calculation was carried out. The relative texture coefficient ($RTC_{(hkl)}$) of 4 peaks namely (111), (200), (220) and (311) of all coated samples were calculated by using equation (2).[12]

$$\mathrm{RTC}_{(hkl)} = \frac{I_{(hkl)}/I_{0(hkl)}}{\Sigma I_{(hkl)}/I_{0(hkl)}} \times 100\%, \tag{2}$$

where $I_{(hkl)}$ is the intensity obtained from textured sample and $I_{0(hkl)}$ the intensity of the standard oriented sample, i.e., from JCPDS data. The obtained RTC values of all the

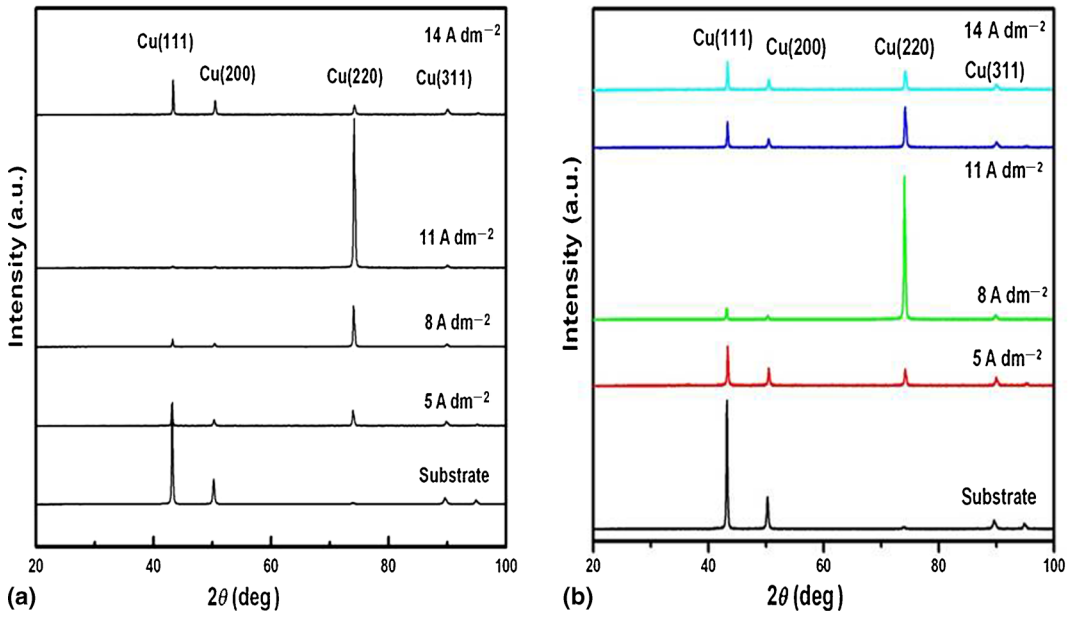

Figure 4. XRD pattern of Cu–TiO_2 composite coatings obtained with (**a**) 10 g l^{-1} TiO_2 and (**b**) 30 g l^{-1} TiO_2 in the bath along with Cu substrate.

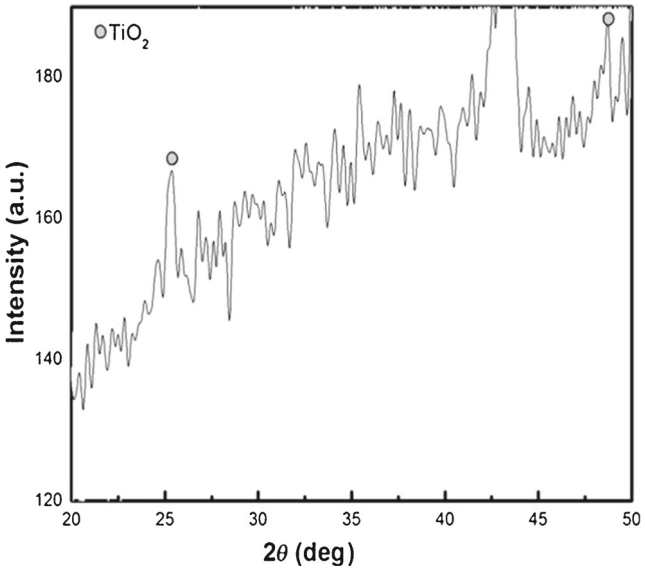

Figure 5. Enlarged XRD pattern of Cu–TiO_2 coating with 10 g l^{-1} TiO_2 and 8 A dm^{-2} current density.

samples are displayed in table 2. The RTC value of each plane should ideally be 0.25 if the material shows totally random orientation. From table 2, it can be observed that in case of pure Cu coating with lower current density (5 and 8 A dm^{-2}) the obtained prominent peak is (220), but at mid-value (11 A dm^{-2}) it shifts towards (111) which contains more strain energy as angle between (111) and (100) is more compared to that of (220) and (100).[13] The RTC value of (220) first increases with the increase in current density followed by a drop. In case of Cu–TiO_2 composite coating also similar trend in RTC of (220) was observed both in case of 10 and 30 g l^{-1} TiO_2 concentration. When the effect of different loadings of TiO_2 on the RTC was done, it was observed that except 11 A dm^{-2}, with increase in TiO_2 content there is a shift from prominent (220) to (111) and (311) mixed orientation. From the discussions on texture study of Cu–TiO_2 system it can be concluded that the observed texture is due to the influence of current density and embedded second phase ceramic particles.

3.4 *Microstructural characterization*

Figure 6 shows FESEM surface micrographs of the electrodeposited Cu–TiO_2 composite coatings prepared with 10 and 30 g l^{-1} TiO_2 concentration bath at current densities of 5 and 11 A dm^{-2}. It can be observed from the figure that with change in current density the deposition morphology changes. Deposit with current density 11 A dm^{-2} looks denser and finer (figure 6b) compared to the same deposited with current density 5 A dm^{-2} (figure 6a). Similar result was also observed in case of Cu–30 g l^{-1} TiO_2 with current density 5 and 11 A dm^{-2} (figure 6c and d). In general, as current density increases the coating becomes denser. High current density creates high over potential and a high over potential is directly proportional to high nucleation rate resulting in denser coating. It can also be observed from figure 6 that, with lower current density (5 A dm^{-2}) the sample appears porous, spongy, poorly adherent and rough (figure 6a and c) compared to their counterparts of higher current density (11 A dm^{-2}) (figure 6b and d). Coating obtained with current density which is lower than a limiting value is inappropriate and thus industrially values near 8 A dm^{-2} is used. But small micropits were observed on surface of the deposited samples obtained with a higher current density. This may be because

Table 2. Relative texture coefficient ($RTC_{(hkl)}$) of different coatings and substrates.

Sample type	Sample details	$RTC_{(hkl)}$% (111)	(200)	(220)	(311)	Crystallite size (nm)
Cu deposition	5 A dm^{-2}	2	1	90	7	41
	8 A dm^{-2}	1	1	95	3	56
	11 A dm^{-2}	51	14	19	16	53
	14 A dm^{-2}	6	8	74	12	64
Cu–TiO_2 coating	10 g l^{-1}, 5 A dm^{-2}	22	13	41	24	50
	10 g l^{-1}, 8 A dm^{-2}	3	2	88	7	65
	10 g l^{-1}, 11 A dm^{-2}	0	0	98	2	57
	10 g l^{-1}, 14 A dm^{-2}	26	22	30	22	65
	30 g l^{-1}, 5 A dm^{-2}	20	17	40	23	65
	30 g l^{-1}, 8 A dm^{-2}	2	1	95	2	76
	30 g l^{-1}, 11 A dm^{-2}	9	5	75	11	51
	30 g l^{-1}, 14 A dm^{-2}	16	11	59	14	41

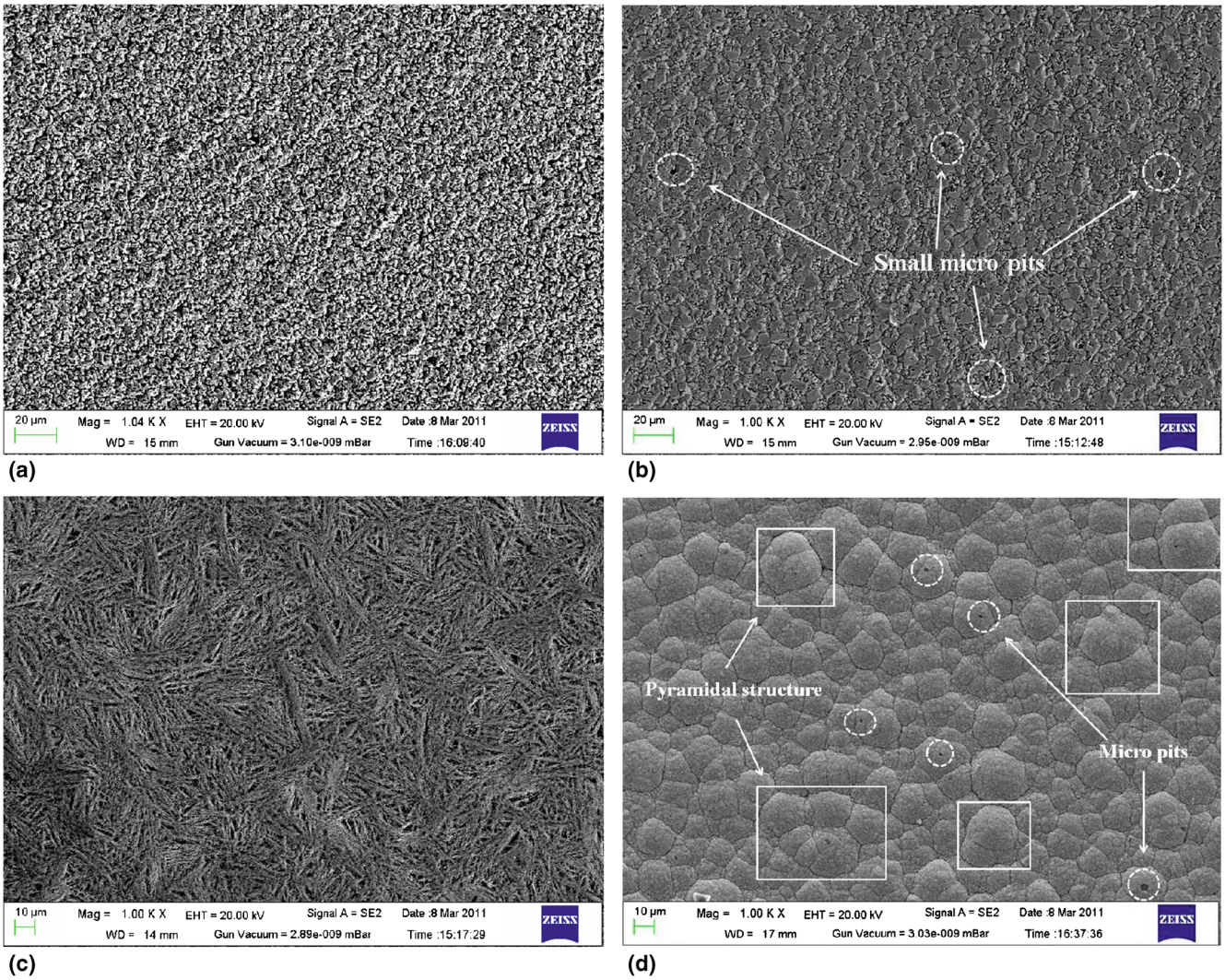

Figure 6. Surface morphology of electrodeposited Cu–TiO_2 coatings: (**a**) 10 g l^{-1} TiO_2 with 5 A dm^{-2}, (**b**) 10 g l^{-1} TiO_2 with 11 A dm^{-2}, (**c**) 30 g l^{-1} TiO_2 with 5 A dm^{-2} and (**d**) 30 g l^{-1} TiO_2 with 11 A dm^{-2}.

Figure 7. EDS of Cu–10 g l^{-1} TiO_2 deposited sample at 5 A dm^{-2}.

of hydrogen evolution at the cathode surface due to over voltage. At 30 g l^{-1} TiO_2 with 5 A dm^{-2} current density the surface morphology of the coating was observed as rope-like structure with void space and loosely compacted on the surface, which was completely different compared to the other micrographs of the Cu–TiO_2 coatings. At 30 g l^{-1} TiO_2 with current density 11 A dm^{-2} the micrograph shows cauliflower-like structure and also some of them were observed pyramidal (smaller cauliflower- or colony-like grains are agglomerated and formed larger cauliflower or pyramid like) structure with well-defined grain boundaries.

3.5 *EDS analysis*

Figure 7 shows the energy-dispersive spectrum of Cu–10 g l^{-1} TiO_2-coated surface developed with 5 A dm^{-2} current density. It is evident from the figure that Ti was present in the composite coating along with copper and oxygen. From the stoichiometry of TiO_2 and the wt% of Ti obtained from the EDS of each coating, TiO_2 content can be estimated. This estimation is highly required as higher bath concentration of TiO_2 does not warrant higher loading in the actual coating in the same ratio. Figure 8 shows the effect of bath composition and deposition parameter on the Ti content of the coatings. From the figure it can be observed that a sharp increase in Ti (so TiO_2) content with increase in bath TiO_2 composition. This is due to increased amount of TiO_2 supply to the cathode region as the amount of TiO_2 increases in the plating bath. The present result is in well agreement with literature, which was reported earlier.[14] In other words, a higher concentration of TiO_2 particulates in the electrolyte enhanced the adsorption rate, thus resulting in a higher weight percentage of the codeposited TiO_2 nano-particulates in the coating. However, the increase in the amount of co-deposited titania particles is not quantitatively comparable with the amount of particles charged to the electrolyte. For example, by increasing thrice the amount of TiO_2 in bath from 10 to 30 g l^{-1}, the particle concentration in the deposited layer was increased only by twice. The co-deposition of TiO_2 nanoparticles on the cathode surface was suggested by Guglielmi's two-step adsorption model.[14] According to this model in the first step the particles are loosely adsorbed on the cathode surface due

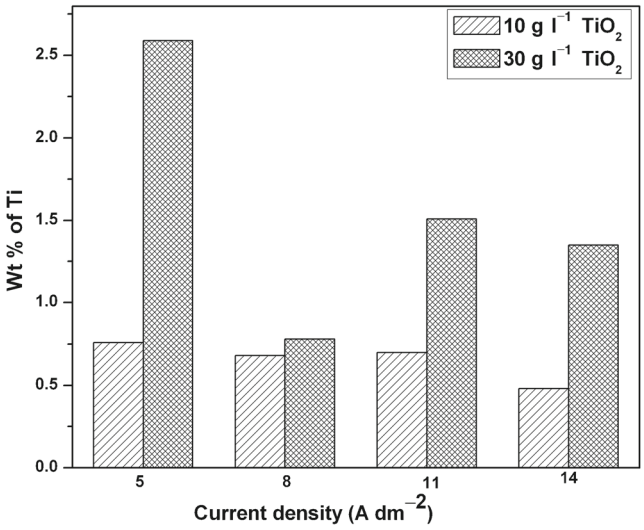

Figure 8. Ti wt% in deposited samples *vs*. TiO_2 concentration in bath at different current densities (5, 8, 11 and 14 A dm^{-2}).

to the weak van der Waal forces, and in the second step the particles are strongly adsorbed on the cathode surface due to the Columbic attractive forces acting between the cathode surface and the anions adsorbed on the particles, then consequently the particles are encapsulated in the growing metal matrix. From the figure variation of Ti with current density is also visible. At all current density values there is less deviation in Ti content when 10 g l^{-1} bath was used. In case of 30 g l^{-1} bath there is actually a decreasing trend in the Ti content in the coating and at 8 A dm^{-2} current density is lowest. At higher current density the main current carrying medium is the metallic ion, not the ion adsorbed oxide particles due to their bulky size. This lead to no improvement in Ti content when the oxide concentration of the bath is raised to 30 g l^{-1}.

3.6 *Microhardness study*

Figure 9 shows microhardness data of all the deposited samples in terms of variation of current density and bath concentration. Briefly the figure tells that the hardness values obtained for the composite coatings (Cu–TiO_2) are higher

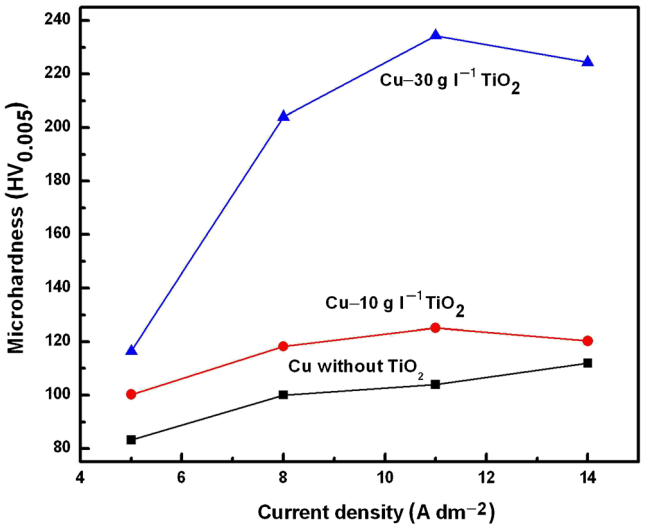

Figure 9. Microhardness of all Cu–TiO_2 coating at different current densities.

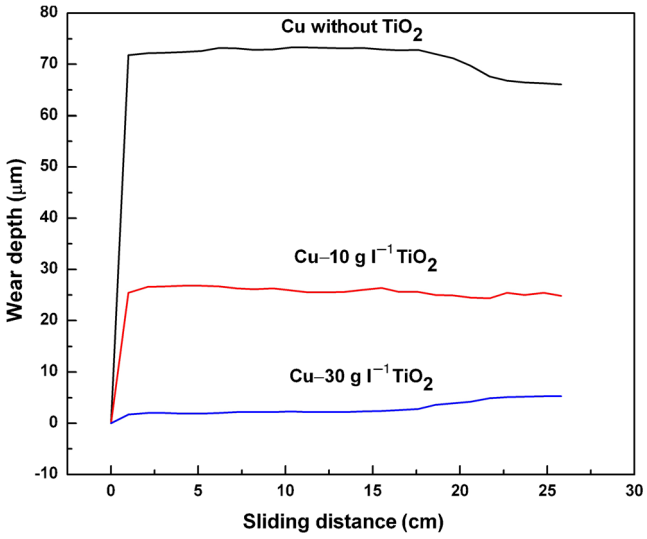

Figure 10. Wear plots of Cu–30 g l^{-1} TiO_2, Cu–10 g l^{-1} TiO_2 and pure copper coating at 11 A dm^{-2} current density.

than pure copper coating and in general it increases with increase in current densities and bath concentration. The current result was also in same trend with other composite coating, which was reported earlier.[15] The compactness of the structure can also be attributed for better hardness at higher current densities as discussed in microstructural characterization section (figure 6). Moreover the crystallite size has limited effect on microhardness values as the sizes are in similar range (table 2).

When figure 9 was analysed minutely, it was observed that in some cases there was mild drop in hardness with increase in current density values and moreover the hardness increase is not exactly in line with the TiO_2 content of the coating (figure 8). In case of pure Cu coating at 11 A dm^{-2} and in case of composite coating with 10 g l^{-1} bath at 14 A dm^{-2}, the hardness values slightly decrease. This may be due to the increase in intensity of (200) plane as this may be corelated with [100] texture associated to deposits with minimum hardness and maximum ductility.[16] The minimum hardness for (200) diffraction line is attributed to lower angle between (200) and (100) planes, which leads to lower strain energy, the strain energy increases as the angle increases.[17,18] In case of 30 g l^{-1} coating at 14 A dm^{-2} similar drop was observed. In case of 30 g l^{-1} bath, though the TiO_2 loading in the coating decreases with increase in current density, there is no such effect in the hardness. This is attributed to the fact that at higher current density (220) + (311) mixed preferred orientations were observed which are known as harder orientations.

Generally the strengthening mechanism of polycrystalline metals, alloys and MMCs are mainly due to grain refinement strengthening by Hall–Petch relationship, dispersion strengthening due to Orowan mechanism and solid solution strengthening. In the present study the positive hardness values observed were mainly due to the dispersion strengthening by the dispersed second phase particles, preferred crystallographic orientation (texture) of the matrix phase and marginal effect of grain size.

3.7 *Wear study*

Figure 10 shows the comparable wear loss graphs (in terms of vertical penetration of the indenter or wear depth) as a function of sliding distance of Cu–10 g l^{-1} TiO_2, Cu–30 g l^{-1} TiO_2 and copper without TiO_2 coating deposited with 11 A dm^{-2} current density. According to the obtained results, it can be said that wear loss is high for pure copper (without TiO_2 particles) coating followed by Cu–10 g l^{-1} TiO_2 and Cu–30 g l^{-1} TiO_2 deposited samples, respectively. Main reason of this type of wear performance is attributed towards dispersion strengthening due to the presence of second phase ceramic oxide particles and same was reported earlier.[19,20] Wear loss of without TiO_2 samples was higher than Cu–10 g l^{-1} TiO_2 and Cu–30 g l^{-1} TiO_2 composite coatings at all current densities due to the absence of dispersed hard ceramic oxide particles. Other strengthening mechanisms as discussed in hardness study are responsible for better performance. In case of some graphs momentary negative slope could be observed. This may due to cold welding or incipient fusion of soft Cu phase with the hardened steel ball (indenter), resulting in decrease in the wear depth. In general it can be concluded that, with increase in ceramic powder contents, the wear resistance of Cu coating increases.

Figure 11 shows the SEM images of the worn surfaces of wear tested samples. Figure 11a and b shows the overall wear track of the worn wear surfaces where as figure 11c and d shows the same wear track at higher magnification of pure Cu coating without oxide powder and Cu–10 g l^{-1} TiO_2 at 11 A dm^{-2} current density. From the figure it can be seen that in case of pure copper coating the wear track depth and width is huge. This can be attributed to the inherent ductility and

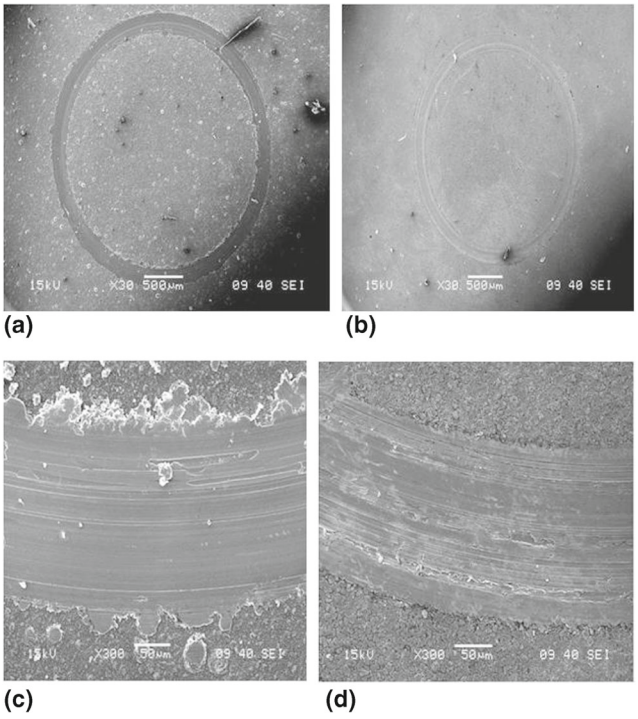

Figure 11. SEM micrographs of wear track of (**a**) pure copper coating (without ceramic oxide), (**b**) Cu–10 g l^{-1} TiO_2 coating at 11 A dm^{-2} current density and (**c** and **d**) micrographs of same wear tracks at higher magnification, respectively.

softness of the copper. Less depth and width were observed in case of Cu–10 g l^{-1} TiO_2 deposited sample. At higher magnification, adhesive nature of wear mechanism is clear for pure Cu coating. But the wear scar with ceramic oxide particles embedded surface shows (figure 11d) more rubbing mark due to three body motion (abrasion by the worn out ceramic particles). It can be concluded that though addition of ceramic oxide in coating increases the wear properties, it marginally transforms the wear nature from adhesive to abrasive type.

4. Conclusions

The present study deals with successful deposition of Cu–TiO_2 composite coating on copper substrate with variation in current densities as well as concentration of ultrafine TiO_2 powder in bath solution. Following conclusions may be drawn:

(a) XRD study shows the development of crystallographic orientation of the Cu matrix as a function of TiO_2 content and deposition parameter.
(b) Different surface morphologies were observed with different current densities and the TiO_2 content in the deposit was not exactly proportional to that of bath concentration.
(c) Positive hardness and wear values resulted in case of Cu–TiO_2 system but the strengthening mechanisms were mainly due to dispersion hardening and preferred crystallographic orientation.
(d) Addition of ceramic oxide in coating increases the wear properties, but it marginally transforms the wear nature from adhesive to abrasive type.
(e) This process may be employed to increase surface mechanical properties of Cu items.

Acknowledgement

Partial financial support for this work from the Council of Scientific & Industrial Research, India (Grant no. 22/0563/11/EMR-II) is gratefully acknowledged.

References

1. Dieter G E 1988 *Mechanical metallurgy* (Singapore: McGraw Hill)
2. Durney L J 1985 *Electroplating engineering handbook* (Van Nostrand Reinhold Company) 4th ed, pp 364
3. Boonyongmaneerat Y, Saengkiettiyut K, Saenapitak S and Sangsuk S 2009 *Surf. Coat. Technol.* **203** 3590
4. Gurrappa I and Binder L 2008 *Sci. Technol. Adv. Mater.* **9** 043001 (pp 1)
5. Low C T J, Wills R G A and Walsh F C 2006 *Surf. Coat. Technol.* **201** 371
6. Lee H K, Lee H Y and Jeon J M 2007 *Surf. Coat. Technol.* **201** 4711
7. Gul H, Kilic F, Aslan S, Alp A and Akbulut H 2009 *Wear* **267** 976
8. Stojak J L, Fransaer J and Talbot J B 2002 In *Advances in Electrochemical Science and Engineering* (eds) Alkire R C and Kolb D M (Weinheim: Wiley-VCH Verlag)
9. Saha R K and Khan T I 2010 *Surf. Coat. Technol.* **205** 890
10. Rashidi A M and Amadeh A 2008 *Surf. Coat. Technol.* **202** 3772
11. Stankovic V D and Gojo M 1996 *Surf. Coat. Technol.* **81** 225
12. Lajevardi S A and Shahrabi T 2010 *Appl. Surf. Sci.* **256** 6775
13. Zhang J M, Zhang Y and Xu K W 2005 *J. Cryst. Growth* **285** 427
14. Ramalingam S, Muralidharan V S and Subramania A 2009 *J. Solid State Electrochem*. **13** 1777
15. Thiemig D, Lange R and Bund A 2007 *Electrochim. Acta* **52** 7362
16. Singh D K and Singh V B 2011 *J. Electrochem. Soc.* **158** 114
17. Zhang J M, Zhang Y, Xu K W and Ji V 2008 *Mater. Lett.* **62** 1328
18. Wang J F, Ma D Y, Xu K W and Liu M 2010 *Adv. Mater. Res.* **609** 89
19. Hou K H, Ger M D, Wang L M and Ke S T 2002 *Wear* **253** 994
20. Aruna S T, William Grips V K and Rajam K S 2009 *J. Alloys Compd.* **468** 546